



United States Department of the Interior

GEOLOGICAL SURVEY
BOX 25046 M.S. 403
DENVER FEDERAL CENTER
DENVER, COLORADO 80225-0046

IN REPLY REFER TO:

February 1, 1988

MEMORANDUM

TO: Ray Wallace, USGS Geothermal Energy Coordinator

FROM: Fred Paillet, Borehole Geophysics Research Project, MS 403

SUBJECT: Final revised copy of MIT manuscript on acoustic velocities of SSSDP core samples

Enclosed is the "final" version of the MIT paper on their results from the acoustic measurements on core samples from the SSSDP. The paper has been accepted by JGR, and will be published in the special SSSDP issue.

The paper on logging by myself and Roger Morin has just been returned from JGR with the reviewers comments. The comments are quite favorable so far as the technical content is concerned, but we will apparently have to undertake a major reorganization to satisfy the editor, who would rather see things get presented in a different order. In any event it seems that the paper will be easily accepted after those revisions. It should take about a month. I will make sure you get a copy when we send the revision back to JGR.

In the meantime, our plans to keep the geothermal truck in order have been foiled by the collapse of the deep Puerto Rican corehole. That would have been of interest to WRD, but our primary concern was to keep the geothermal logging truck in good working condition so as to avoid the "rust and dust" problems we had gearing up for the SSSDP. The Puerto Rico project may continue by rebidding the drilling later on, but right now we are still looking for a place to exercise the truck and equipment. Any suggestions?

Best wishes for the new year, etc.

Laboratory Studies of the Acoustic Properties of Samples
from the Salton Sea Scientific Drilling Project and Their
Relation to Microstructure and Field Measurements

P.A. TARIF, R.H. WILKENS¹ AND C.H. CHENG

Earth Resources Laboratory, Department of Earth, Atmospheric and Planetary Sciences

Massachusetts Institute of Technology, Cambridge, Massachusetts 02139.

F.L. PAILLET

Borehole Geophysics Research Project, USGS/WRD, Denver, Colorado

Submitted to the Journal of Geophysical Research

Revised December, 1987

¹ Now at Hawaii Institute of Geophysics, Honolulu, Hawaii 96822.

Abstract

Compressional and shear wave velocities were measured at confining pressures up to 200 MPa for twelve core samples from the depth interval of 600 to 2600 m in the California State 2-14 borehole. Samples were selected to represent the various lithologies, including clean, heavily cemented sandstones, altered, impermeable claystones, and several intermediate siltstones. Velocities measured at ultrasonic frequencies in the laboratory correspond closely with velocities determined from acoustic waveform logs and vertical seismic profiles. The samples exhibit P-wave velocities around 3.5 *km/sec* at depths above 1250 m, but increase to nearly 5.0 *km/sec* at 1300 m in depth. Further increases with depth result in compressional wave velocity increasing to nearly 6.0 *km/sec*. These increases in velocities are related to systematic variations in lithology, microstructure and hydrothermal alteration of originally clay-rich sediments. Scanning electron microscope observations of core samples confirm that local core velocities are determined by the combined effects of pore size distributions, and the proportion of clays and alteration minerals such as epidote present in the form of pore fillings and veins.

Introduction

The Salton Sea Trough is an active tectonic depression that has been collecting sediments from the adjacent Colorado River Delta for thousands of years. It is located at the junction of the active extensional rift of the Gulf of California and the transform faults of Southern California. The geothermal gradient throughout the area is anomalously high. Thus the Salton Sea Trough provides a perfect setting for studying how the sediments in the basin are altered by the high temperatures and hydrothermal circulation. The primary objective of the laboratory study of cores from the State 2-14 borehole at the edge of the Salton Sea was the development of an understanding of the relationship between such core properties as local mineralization and pore size spectra and compressional and shear wave velocities. An in-depth understanding of the velocity-lithology relationship is especially important in analysis of data from the 3250 m deep State 2-14 borehole of the Salton Sea Scientific Drilling Project because both vertical seismic profiles and acoustic logs are available. Although ultrasonic laboratory measurements provide comparison velocities for a limited number of samples, examination of such velocity data and the microscopic structure of core lithologies yields important insight into the relationship between lithology and velocity throughout the borehole. These results are subsequently used in the evaluation of velocity distributions given by acoustic waveform logs and vertical seismic profiles. The data suggest how the extent of hydrothermal alteration and core mineralization over the total depth of the borehole are reflected in velocity variations measured at several scales.

The State 2-14 borehole was drilled as part of a major scientific study of the Salton Sea Geothermal reservoir. Seismic data at various scales of investigation were intended to provide indications of

geothermal reservoir properties (pressure, porosity, and permeability) and indications of geothermal activity (alteration and mineralization). The increase in seismic velocity associated with increasing confining and effective pressure in laboratory studies is well known [Toksöz *et al.*, 1976; Todd and Simmons, 1972; Nur and Simmons, 1969]. Various theories can be used to relate such increases in velocity with pressure to the spectrum of pore shapes and microfractures within the rock fabric [Cheng and Toksöz, 1979; O'Connell and Budiansky, 1977]. The experimental results obtained when subjecting individual rock samples to increasing pressures may be seen as a partial analog to increases of velocity with depth, as it is expected that fewer thin cracks remain open as pressure increases. In practice, closing of cracks with depth is often accomplished through chemical alteration rather than mechanical pressure, and might more reasonably be termed crack filling. At the State 2-14 borehole the extreme temperature gradient also complicates the analogy since temperature increases generally decrease velocities in opposition to the pressure effect.

The one important effect of *in situ* conditions on acoustic propagation that is not indicated by the ultrasonic velocities determined from core samples is the effect large-scale fractures have on measured seismic velocities. Open or partially open fractures reduce the mechanical strength of rocks, reducing seismic velocities and increasing attenuation. Intact cores are often not recovered from fractured zones, and experimental methods require relatively sound samples to withstand the processing required to produce specimens of the proper dimension for testing. The comparison between predicted velocities for intact samples of representative lithologies in the State 2-14 borehole given as a function of *in situ* confining pressure provide an important means for separating velocity anomalies associated with varying lithologies from those produced by the presence of fractures in

the geothermal reservoir.

Selection and Preparation of the Samples

Because ultrasonic core velocity measurements were used to relate the microscopic structure of a limited number of discrete samples to the macroscopic velocity structure given by well logs and vertical seismic profiles, sample selection was a critical factor in the completion of this study. Fourteen samples, evenly distributed over the depth intervals of core available, were selected to represent the full spectrum of lithologies. Sample selection was made on the basis of visual core description given by *Mehegan et al.* [1986] and checked against geophysical log data given by *Paillet* [1986]. The depths and visual descriptions of the fourteen samples are given in Table I. Among these fourteen samples, seven can be considered as lithologic endpoints based on quartz content: samples from depths of 1060, 1837 and 2226 m for the claystone and shale group, and 954, 1170, 1305, and 2618 m for the sandstone group (the names of the samples in further discussion will correspond to their *in situ* depths).

Individual samples for ultrasonic testing were prepared by cutting 2.5 cm diameter cylinders from sections of the core. Measurements of seismic velocities of stratified Salton Sea sediments may show differences between measurements parallel and transverse to bedding planes, even after hydrothermal alteration. For this reason, cores were processed to allow velocity measurement transverse to bedding for comparison with velocities of vertically polarized shear waves measured in vertical seismic profiles, and seismic velocities determined from acoustic waveform logs. For seven of the selected depths sample cylinders were cored with their axes parallel to the axis of the well.

Otherwise, they were cored with axes perpendicular to the axis of the well. The ends of the cores were cut using a precision wafering saw which produced flat surfaces suitable for the velocity tests. Lengths of the samples ranged between 12 mm and 50 mm, depending primarily on the friability of the rock. Due to the abundance of cracks in certain well-cores, it was impossible to prepare any sample longer than 12 mm.

The effective porosity and bulk density of the cores were calculated from the weights of each core after oven drying, saturation with water, and immersion in water. Dry measurements were made after the samples had been baking in a vacuum oven at 60 °C for two days. Saturated measurements were made after immersion of the dry samples in degassed water under vacuum for 24 hours and then under atmospheric pressure for 24 hours. The shaley samples were re-weighed after testing in order to insure that their grain densities and porosities had not changed due to saturation with fresh water pore fluid. Sample volumes were obtained by weighing fully saturated in water.

The measured properties of the samples are summarized in Table II. The data clearly show an increase in the saturated bulk density with increasing depth, reflecting mainly a decrease in porosity (Figure 1). Effective porosities range between 3.1% and 24.1%. Porosity versus bulk density is presented in Figure 2. Theoretical straight lines have been calculated for media of varying porosities and grain-densities. The position of each sample provides the reader with an indication of its average grain-density. Although a small residual amount of porosity may not be measured by immersion techniques, previous studies have shown that this error is small in sandstones and shaley clastics [Caruso *et al.*, 1985]. The average grain-density gives a first rough

idea of the mineralogical composition of the samples; for instance, a clean quartz sandstone would lie on the theoretical line of grain-density 2.65 g/cm^3 . The averaged grain-densities of the samples have been listed in Table II; all but sample 1984 lie in the range 2.62 to 2.79 g/cm^3 .

Velocity Measurements

Compressional and shear wave velocities were measured under varying hydrostatic confining pressure on dry and saturated samples. As widely recognized in the literature [for example, *Wyllie et al.*, 1958; *Todd and Simmons*, 1972], the effects of *in situ* state of stress on the physical properties of a given rock can be described by taking into account only the effective pressure, which is defined as the difference between the confining pressure and the pore fluid pressure. In the measurements described here, effective stress was controlled by draining the samples without dissicating clay minerals, setting the pore pressure at atmospheric pressure and recording measurements as a function of confining pressure.

Two 500 kHz piezoelectric crystals were used to record transmitted ultrasonic signals through the samples. Each of them is protected from the confining pressure in a steel case, and a steel buffer 37.5 millimeters thick separates each transducer from the sample. A neoprene jacket isolates the pore space from the pressurized kerosene.

Table II summarizes the data collected for the fourteen samples. Measurements were made on the same samples during repeated pressure cycles. Compressional and shear wave velocities are reported for two pressures: 200 MPa and the calculated *in situ* pressure. The first value is an estimate of the effective pressure experienced by the sample *in situ*, calculated assuming an average

rock density of 2.45 g/cm^3 for the sedimentary column and 1.00 g/cm^3 for the pore fluid. The second value is the velocity at the maximum confining pressure attainable with our experimental set-up. The relation between ultrasonic velocities at *in situ* pressure and depth for all the samples is shown in Figure 3. Temperature was not taken into account although increased downhole temperatures lower velocity values on the order 0.10 to 0.20 km/sec [Peselnick and Stewart, 1975]. This is equivalent to the size of the symbols in most of our plots. The expected trend of increasing velocities with increasing depth is clearly indicated.

Apart from its mineralogy (both grains and cement), the mechanical properties of a sedimentary rock are mainly governed by the volume and the distribution of its pore spaces. A plot of the velocities as a function of the effective pressure yields information about the distribution of this porous volume into various pore-shape factors [Cheng and Toksöz, 1979]. Different relations between the P- or S-wave velocities and the effective pressure are illustrated in Figures 4, 5, 6 and 7. Samples containing relatively larger volumes of low aspect ratio pores (cracks) exhibit larger increases in measured velocity as confining pressure is increased. Sample 911, a very porous, poorly-cemented and highly fractured shallow siltstone exhibits this type of behavior, increasing 0.8 km/sec in P-wave velocity between pressures of 20 and 200 MPa (Figure 4). A highly cemented, low-porosity shale (Sample 1837, Figure 6) has a very small pressure dependence, exhibiting a velocity increase of only 0.25 km/sec over the same interval of confining pressure. The same kind of comparative statement could be made between the shallow sandstone (Sample 1170, Figure 5) and a sandstone recovered from deeper in the hole (2618, Figure 7).

Due to the pressure dependence of the velocities, the influence of the mineralogical composition

is best studied using the data collected at high confining pressure where most of the flat cracks are closed. The value of V_P at 200 MPa confining pressure has been plotted versus the measured porosity of each core in Figure 8. Velocity-porosity curves plotted in this figure were calculated using Wyllie's [1958] time-average relationship for a mono-mineralic rock. The minerals considered here are quartz ($V_P = 6.05 \text{ km/s}$) and epidote ($V_P = 6.96 \text{ km/s}$). The equation states that if V_G is the velocity of compressional waves in the mineral grains and V_W the velocity of compressional waves in the pore-filling fluid, then the velocity of compressional waves V_P in this rock will be written as:

$$\frac{1}{V_P} = \frac{\phi}{V_W} + \frac{1 - \phi}{V_G}$$

where ϕ is the porosity. The time-average equation has been derived from experimental observations made on sandstones; it is not supported by any rigorous theoretical basis. Nevertheless, eight out of the twelve samples for which there are complete set of measurements fall between the two modeled time-average curves.

Discussion

It has been established that both the lithology and the distribution and shapes of pores and cracks determine the variations in the ratio V_P/V_S [for example *Tatham*, 1982]. High ratios suggest a relatively greater abundance of flat cracks in rocks of the same composition. We have plotted the values of V_P/V_S at 200 MPa effective pressure versus V_P/V_S at the *in situ* effective pressure for each fully water-saturated sample in Figure 9. The samples are separated into two classes according to their quartz content (see Table II). Six of the samples are composed primarily of sand sized quartz

grains and thus have been termed sandstones. The other eight samples are either fine grained siltstones and claystones or shales.

There are two interesting aspects of the data displayed in Figure 9. At confining pressures of 200 MPa the range of values for the ratio V_P/V_S is appreciably lower for the sandstones than for the other samples. This is related to the low value of the V_P/V_S ratio of quartz (1.45) compared to most other minerals (1.8–2.0) [Pickett, 1963; Wilkens *et al.*, 1984]. This effect is not evident at the *in situ* pressures, where open cracks seem to dominate the velocity values. In addition, all but one of the high-pressure ratios is smaller than the *in situ* ratios of the same sample. This can be explained by the greater sensitivity of S-waves to the presence of low aspect ratio pore volume, i.e., to the presence of cracks which close as the differential pressure applied to the rock increases. Figure 9 illustrates ways in which both porosity and mineralogical composition have important influence on the mechanical properties of a given rock sample.

Discussion of the SEM Results

The end-cuts from twenty five millimeter diameter cores obtained during the preparation of the samples for the ultrasonic measurements were used to prepare samples for SEM investigations. A first inspection was performed on polished sections of dry samples. Such images show in great detail the three-dimensional geometry of pores. However, it is difficult to get any quantitative analysis of such images. Hence, a second observation was performed on samples fully saturated with epoxy in order to reliably examine the pore geometries and the main mineral-phases on a two-dimensional image. The images shown in Plates 1 through 8 have been obtained with a backscattered electron detector and are presented at the same magnification in each plate. The

response of this detector is proportional to the density of the material which is under the beam. For instance, low-density epoxy will appear black in the pictures, while relatively light silica will appear dark-grey and dense minerals like pyrite will appear bright white. The microscope is also equipped with an Energy Dispersive System which yields quick, low-cost qualitative analyses of all the elements encountered by the beam whose atomic number exceeds eleven. Table III summarizes the results of our observations. Estimations of frequencies with which certain given phases occur in the pictures are given when possible. These estimations result from point counts made on several frames of the sample under scan. Those samples for which no estimation has been given are mainly those which were difficult to fully saturate with epoxy. These were the low-permeability claystones.

The SEM photomicrographs in plates 1 through 8 provide considerable insight into the effects of pore size distributions and mineral composition on seismic velocities of rock samples. These effects may be considered by comparing the SEM photographs for three groups of samples, along with the results displayed in Figures 2 and 8. Groups A and B were chosen to represent samples that exhibited very different velocities while sharing similar porosities. Group C has a different sense; samples of nearly the same velocity that have a wide range of porosities.

Group A: 2618, 1294, 1228

SEM photomicrographs of an epidotized sandstone (2618), a siltstone (1294) and a shale (1228) are shown in Plates 8, 5, and 4. The average grain-density of 2618 stands close to the grain-density of quartz (see Table II and Figure 2) while the grain-density of the two shales is larger, reflecting the presence of clays, whose grain-density is highly variable (for instance, illite: $2.6\text{--}2.9\text{ g/cm}^3$ [Berry *et al.*, 1983]). These three samples have in common a low porosity (from 5.1% to 6.3%), but their

P-wave velocities at 200 MPa differ substantially (0.75 km/sec). The SEM photomicrographs reveal very different textures for the three samples, ranging from the relatively large grain size and open pore spaces in the sandstone (2618) to the fine grain size and small micropores of the shale (1228). Theoretical models (eg. *Kuster and Toksöz* [1974], *Cheng and Toksöz* [1979]) show that the effect of pores on the ultrasonic properties of rocks is a function of the aspect ratio distribution of the porosity. The result is that, in samples of equal porosity, the flatter the pores, the lower the P- and S-wave velocities.

Group B: 1984, 1415, 1060

An epidotized sandstone (1984), an epidotized shale (1415), and a relatively unaltered shale (1060) are presented in Plates 7, 6, and 2. As in the case of Group A, these samples have similar porosities (10.4 % - 11.5 %) but different velocities at 200 MPa (5.30 km/sec - 4.20 km/sec, Figure 8) and the sample with the lowest velocity (1060) also has small, flat pores. Cementation of grains is another important factor in the velocities of these three samples. Sample 1984 has been cemented with epidote. Epidote is a heavy mineral, the density of the more common mineral phases ranging between 3.3 and 3.6 g/cm^3 , which explains the high average grain-density of sample 1984. The presence of epidote, filling the cracks and hardening the rock, is responsible for the greater ultrasonic velocities of sample 1984 (the most epidotized) over sample 1415 (some epidote) and 1060 (no epidote or any other pore-filling material).

Group C: 954, 1170, 1060

Plates 1, 3 and 2 are SEM photomicrographs of a clean sandstone (954), a shaley sandstone (1170) and a shale (1060). The average grain-density of the latter (see Table II and Figure 2) agrees well with the typical values of clay grain-density while the two other samples are close to the grain-density of quartz (2.65 g/cm^3). These three samples, despite their range of porosities (from 13.4% to 21.1%), have very similar ultrasonic P-wave velocities at 200 MPa (4.00 km/sec - 4.20 km/sec, Figure 8). The difference between 1060 (shale) and the two sandstones is another illustration of the greater effect the flat pores have on the decrease of the P-wave velocity. The low porosity shale has more flat pores which result in a velocity similar to the higher porosity sandstone.

The case of the two sandstones is somewhat different. Theoretical models have been developed [Cheng and Toksöz, 1979] and successfully applied to explain the ultrasonic P-wave velocities of sandstones [Wilkins *et al.*, 1986]. They found that concentrations of clays in sandstone pores have little effect on the moduli of the rock, and thus the velocity of that sandstone. The clays do, however, reduce the void volume (porosity) of a sandstone. Thus, samples 954 and 1170 appear to have roughly the same volume of quartz, the mineral that composes their framework and dictates velocity, while 1170 contains clay in the pores, lowering porosity without effect on velocity.

The use of SEM images provided us with qualitative information suitable for explaining the behavior of our samples. Differences can be attributed to mineralogy, microstructure, and alteration. Mineralogy of the framework may influence overall velocities and the presence of quartz is particularly noticeable in V_p/V_s ratios at higher pressures. The role of the microstructure changes with pressure. Some cracks (low aspect ratio pores) appear to remain open at *in situ* pressures based

on a comparison of *in situ* and 200 MPa velocities and velocity ratios. At higher pressures, with most of the finer cracks closed, microstructural effects are more likely to include those of alteration. Clays filling pores, while not substantially changing the velocity of a sample, tend to mask the true volume of the framework of the rock, changing porosity values for samples of similar framework volume. Alteration is also important in the formation of the cement which binds grains together. Small volumes of alteration minerals such as epidote acting as cement may increase velocities in a sample out of proportion to its abundance due to its effect of strengthening the framework of the rock.

Comparison With Other Seismic Velocity Data

The great difference in size between the cores cut for the ultrasonic measurements and the much larger volumes of rock sampled by the conventional acoustic logs and vertical seismic profiles complicate the comparison of different velocity data sets. These scale differences can be illustrated by considering the differences in effective seismic wavelengths under the assumption of a typical compressional velocity of 4.0 km/s. The appropriate frequencies of 500 kHz, 15 kHz, and 200 Hz for the ultrasonic, acoustic log, and vertical seismic profile measurements yield wavelength scales of 0.8 cm, 27 cm, and 20 m respectively. In addition to this great difference in scale, the velocity dispersion introduced by intrinsic attenuation [Sachse and Pao, 1978] makes a close agreement between these various measurements even less likely. The combined effects of velocity dispersion and the elimination of the more friable samples during the sample preparation process are expected to cause the ultrasonic velocity values to average slightly greater than velocities determined *in situ*.

A comparison of compressional wave velocities determined from the high gain full waveform

acoustic log (FWAL, *Paillet and Morin, this issue*), vertical seismic profile (VSP, *Daley et al., 1987*), and our measured core velocities is presented in Figure 10. All three velocities agree well with each other. There are two depths (1228 and 1294 m) where the core velocities are significantly higher than the VSP and FWAL velocities. These two points correspond to places where the cores are highly fractured (especially along bedding planes) and it was difficult to obtain an intact sample. Thus the laboratory samples are more competent than the surrounding rocks in these two areas and consequently, they have higher velocities. The two samples with velocities less than the VSP (910 and 1060) are probably due to local variations; they probably represent slower layers in the stratified column. The VSP velocities are averaged over a 60 m interval [*Daley et al., 1987*] and thus failed to pick up the three thin, low velocity zones at around 1350, 1450 and 1500 m in depth. The VSP does show a decrease in velocity between 1410 and 1470 m, but as expected, does not have the depth resolution of the FWAL. Over an area where the velocity changes are more gradual (1150 to 1320 m) the VSP and FWAL velocities are in excellent agreement.

Figure 11 compares the core measured shear wave velocities with (a) SH and (b) SV velocities determined from VSP [*Daley et al., 1987*]. Except for one core (1294) in this interval, all the velocities are measured in line with the axis of the borehole. Given the relatively shallow dip of bedding through most of this interval, vibration directions for the shear waves were in the bedding planes. In the case of 1294 velocities were measured normal to the axis of the borehole, but with vibration again in the plane of the bedding.. The core measured velocities are in general agreement with the VSP velocities, better with the SH than the SV due to the coincidence of vibration in the two determinations.

The three velocity profiles superimposed in Figure 10 follow a general trend. Velocities are relatively low above 1200 m, and gradually increase over a depth interval from 1150 m to approximately 1320 m. Below this level, while the acoustic log suggests several excursions to lower velocities, VSP velocities remain constant. These rapid increases in V_P and V_S between 1200 m and 1300 m can be related to the major interval of clay mineral transformation discussed in *Paillet and Morin* [this issue]. They correspond to the depth of appearance on the SEM photomicrographs of denser zones. These zones have a K-feldspar composition (see Table III) and constitute bulky homogeneous areas around certain quartz grains. Plate 5 is a good illustration of this phenomenon (see upper left side).

The consistency of the three velocity data sets also indicates the apparent lack of macroscopic fractures above a depth of 2000 m in the State 2-14 well. No indications of major permeable fractures have been found in the geophysical logs for this upper portion of the borehole, and flow tests confirmed the low production of geothermal fluids [*Paillet, 1986*]. Major permeable fractures were encountered at greater depths where borehole conditions precluded acquisition of Vertical Seismic Profiles and waveform log data. Ultrasonic velocities determined from intact core samples below 2000 m in depth would not be expected to indicate the presence of fractures.

Conclusions

The good agreement between the seismic velocities determined from the ultrasonic core tests described here and the velocities given at much larger scales of investigation by the acoustic waveform logs and vertical seismic profiles data help in the interpretation of the *in situ* velocity distribution.

The two individual core samples which yielded velocities slightly greater than those given by the log data can be attributed to the selection for intact specimens in the sample preparation process. All seismic velocity data indicate a transition zone in the interval from 1200 to 1800 m in depth where velocity increases are significantly greater than expected from the normal increase in confining pressure with depth. These increases appear to be associated with the hydrothermal alteration of clay minerals in alluvial sediments, and are consistent with temperature logs given for the State 2-14 borehole by *Paillet* [1986] and the mineralogic zonation for wells in the Salton Sea geothermal field given by *Muramoto and Elders* [1984]. Scanning electron photomicrographs of core samples confirm that the measured ultrasonic velocities represent the combined effects of mineralogy, pore size distributions and alteration minerals. The consistency between all three independently obtained velocity data sets indicates that surface seismic data and acoustic waveform logs can be used to relate observed velocities and the extent of hydrothermal alteration.

Acknowledgements

We would like to thank Tom Daley of the University of California at Berkeley for providing us with the VSP data. This work was supported by USGS grant No. 14-08-001-A-0328. P.A. Tarif was also supported by an Elf-Aquitaine post-doctoral fellowship.

References

Berry, L.G., B. Mason, and R.V. Dietrich, *Mineralogy - concepts, descriptions, determinations*, 2nd ed., W.H. Freeman and Co., San-Fransisco, 1983.

- Caruso, L., G. Simmons, and R. H. Wilkens, The physical properties of a set of sandstones, I: The samples, *Int. J. Rock Mech. Min. Sci. & Geomech. Abstr.*, *22*, 381-392, 1985.
- Cheng, C.H., and M.N. Toksöz, Inversion of seismic velocities for the pore aspect ratio spectrum of a rock, *J. Geophys. Res.*, *84*, 7533-7543, 1979.
- Daley, T.M., T.V. McEvelly, and E.L. Majer, Analysis of VSP Data at the Salton Sea Scientific Drilling Project, *EOS*, *68*, 445, 1987.
- Kuster, G.T., and M.N. Toksöz, Velocity and attenuation of seismic waves in two-phase media: Part I. Theoretical formulations, *Geophysics*, *39*, 587-606, 1974.
- Mehegan, J.M., C.T. Herzig, and R.M. Sullivan, Salton Sea Scientific Drilling Project - California State 2-14 Well - Visual Core Descriptions, Volume 1 and 2, University of California, Riverside, 1986.
- Muramoto, F.S., and W.A. Elders, Correlation of wireline log characteristics with hydrothermal alteration and other reservoir properties of the Salton Sea and Westmorland geothermal fields, Imperial Valley, California, *Los Alamos Scientific Laboratory Report LA-10128-MS*, 100pp, 1984.
- Nur, A., and G. Simmons, The effect of saturation on velocity in low porosity rocks, *Earth Plan. Sci. Lett.*, *7*, 99-108, 1969.
- O'Connell, R.J., and B. Budiansky, Seismic velocities in dry and cracked saturated solids, *J. Geophys. Res.*, *79*, 5412-5426, 1974.

- Paillet, F.L., Preliminary Report on Geophysical Well-Logging Activity on the Salton Sea Scientific Drilling Project, Imperial Valley, California, *U.S. Geological Survey, Open-File Report 86-544*, Denver, CO 80225, 1986.
- Paillet, F.L., and R.H. Morin, Analysis of geophysical well logs obtained in the State 2-14 borehole, Salton Sea Geothermal Area, California, *this issue*, 1987.
- Peselnick, L. and R.M. Stewart, A sample assembly for velocity measurements of rocks at elevated temperatures and pressures, *J. Geophys. Res.*, *80*, 3765-3768, 1975.
- Pickett, G.R., Acoustic character logs and their application in formation evaluation, *J. Petr. Tech.*, 659-667, 1963.
- Sachse, W., and Y.H. Pao, On the determination of phase and group velocities of dispersive waves in solids, *J. Appl. Phy.*, *49*, 4320-4327, 1978.
- Tathman, R.H., V_P/V_S and lithology, *Geophysics*, *47*, 336-344, 1982.
- Todd, T., and G. Simmons, Effect of pore pressure on the velocity of compressional waves in low-porosity rocks, *J. Geophys. Res.*, *77*, 3731-3743, 1972.
- Toksöz, M.N., C.H. Cheng, and A. Timur, Velocities of seismic waves in porous rocks, *Geophysics*, *41*, 621-645, 1976.
- Wilkins, R.H., G. Simmons, T.M. Wissler, and L. Caruso, The physical properties of a set of sandstones - Part III. The effects of fine-grained pore-filling material on compressional wave velocity, *Int. J. Rock Mech. Min. Sci. & Geomech. Abstr.*, *23*, 313-326, 1986.

Wilkens, R.H., G. Simmons, and L. Caruso, The ratio V_P/V_S as a discriminant of composition for siliceous limestones, *Geophysics*, 49, 1850–1860, 1984.

Wyllie, M.R.J., A.R. Gregory, and G.H.F. Gardner, An experimental investigation of factors affecting elastic wave velocities in porous media, *Geophysics*, 23, 459–493, 1958.

Figure Captions

Figure 1: Wet bulk density and measured porosity for all the core samples as a function of their *in situ* depths.

Figure 2: Wet bulk density for all the core samples versus their measured porosity. The straight lines have been calculated for porous media of grain densities between 2.4 and 3.

Figure 3: V_P and V_S for all the core samples fully saturated with water at the *in situ* effective pressure as a function of their *in situ* depth.

Figure 4: V_P and V_S of siltstone sample 911 fully saturated with water as a function of effective pressure.

Figure 5: V_P and V_S of sandstone sample 1170 fully saturated with water as a function of effective pressure.

Figure 6: V_P and V_S of shale sample 1837 fully saturated with water as a function of effective pressure.

Figure 7: V_P and V_S of sandstone sample 2618 fully saturated with water as a function of effective pressure.

Figure 8: V_P at 200 MPa effective pressure versus measured porosity for all the core samples fully saturated with water.

Figure 9: V_P/V_S ratio at 200 MPa effective pressure versus V_P/V_S ratio at the *in situ* effective pressure.

Figure 10: Compressional velocities determined from maximum gain FWAL (small dot), VSP (line, from *Daley et al.*, [1987]) and ultrasonic core measurement (black diamond).

Figure 11: (a) SH and (b) SV velocities determined from VSP [*Daley et al.*, 1987]. Ultrasonic core shear velocities are plotted (black square) on both.

Plate Captions

Plate 1: Sample 954. Depth: 954.5 m. Mag 40. Scale bar = 1 millimeter. Scanning electron microscope photomicrograph of backscattered electron image. Black: empty pores filled with epoxy. Dark grey: quartz grains. Light grey: potassic feldspar, clay.

Plate 2: Sample 1060. Depth: 1060.2 m. Mag 100. Scale bar = 100 μ . Scanning electron microscope photomicrograph of backscattered electron image. Black: Holes left by plucked grains (most certainly quartz). Dark grey: quartz grains. The bulk of the rock is mainly made of clays.

Plate 3: Sample 1170. Depth: 1170.2 m. Mag 60. Scale bar = 100 μ . Scanning electron microscope photomicrograph of backscattered electron image. Black: empty pores. Dark grey:

quartz grains. Light grey: plagioclase feldspar, clay. White: Heavy minerals such as pyrite, epidote, calcite.

Plate 4: Sample 1228. Depth: 1228.4 m. Mag 200. Scale bar = 100 μ . Scanning electron microscope photomicrograph of backscattered electron image. Dark grey: quartz grains. White: pyrite. The bulk of the rock is mainly clays.

Plate 5: Sample 1294. Depth: 1294.2 m. Mag 60. Scale bar = 100 μ . Scanning electron microscope photomicrograph of backscattered electron image. Dark grey: quartz grains. White: pyrite (massive crystal center-left), halite crystals covering the walls of the pores. An important fraction of the rock is clay.

Plate 6: Sample 1415. Depth: 1415.9 m. Mag 60. Scale bar = 100 μ . Scanning electron microscope photomicrograph of backscattered electron image. Black: empty spaces (mainly in the veins not totally healed). Dark grey: quartz grains. Light grey: patches of bulky mineral, the composition of which is the composition of potassic feldspar (probably clay). White: epidote, filling the cracks (and then crystallizing in large euhedral shapes), or filling the pore spaces throughout the sample. Crossing the field of the image, from the top-left to the lower-right, a crack totally free of any trace of healing suggests a non *in situ* origin.

Plate 7: Sample 1984. Depth: 1984.6 m. Mag 100. Scale bar = 100 μ . Scanning electron microscope photomicrograph of backscattered electron image. Dark grey: quartz grains. Light greys: clays and empty pores. White: epidote, filling the cracks (upper-left), or the pore space throughout the sample. For this sample, the full saturation with epoxy has been

difficult to reach, hence the bad visualization of the pore space.

Plate 8: Sample 2618. Depth: 2618.4 m. Mag 72. Scale bar = 100 μ . Scanning electron microscope photomicrograph of backscattered electron image. Black: empty pores (here filled with epoxy). White: mainly epidote, some crystals of rutile. Grey: quartz. We can distinguish between grains having a plain aspect and those having a mottled texture, suggesting different origins.

| Depth (m) | Depth (ft) | Unit | Description Mineralogy |
|--------------|---------------|-------|---------------------------------------------------------------------------------------------------------------------------|
| 606.2 | 1988.7 | 13.1 | Very fine-grained, light-grey mudstone Microcrystalline clay |
| 911.0 | 2988.7 | 37b.4 | Fine-grained green sandstone with interbedded siltstone Quartz, clay, feldspar |
| 954.5 | 3131.5 | 69.1 | Light green-grey sandstone Quartz, feldspar |
| 1060.2 | 3478.5 | 86.1 | Light-green calcareous thinly laminated siltstone Muscovite, clay, quartz |
| 1170.2 | 3839.2 | 114.1 | Light grey-green medium-grained sandstone Quartz, black lithics, muscovite |
| 1228.4 | 4030.1 | 128.1 | Medium-dark-grey laminated shale Clay, quartz |
| 1294.4 | 4245.9 | 144.1 | Medium-grey laminated siltstone Clay, quartz |
| 1305.7 | 4283.8 | 159.1 | Green fine-grained sandstone, interbedded grey siltstone Quartz, feldspar, clay |
| 1320.1 | 4331.0 | 175.1 | Medium-grey laminated shaley siltstone Clay |
| 1415.9 | 4645.5 | 182.1 | Grey-green laminated siltstone Clay |
| 1837.1 | 6026.8 | 220.1 | Medium to dark-grey shale Clay. Silicified appearance. |
| 1984.6 | 6511.0 | 228.1 | Green, fine-grained sandstone, interbedded coarse siltstone Clays, quartz, recrystallization signs, epidote throughout |
| 2226.6 | 7305.0 | 245.1 | Grey-green siltstone Clay, quartz |
| 2618.4 | 8590.5 | 289.1 | Light-green fine-grained massive sandstone Quartz |

Table I - Description and mineralogy of the samples as given in the visual core description [Mehegan *et al.*, 1986].

| Depth (m) | Depth (ft) | Wet dens. g/cm^3 | porosity % | grain dens. g/cm^3 | A | B | C | D | E | F | G | H | I | J |
|-----------|------------|--------------------|------------|----------------------|------|------|------|------|------|------|------|------|---|---|
| 606.2 | 1988.7 | 2.32 | 24.1 | 2.74 | | | | | 2.40 | 3.90 | | | 0 | 0 |
| 911.0 | 2988.7 | 2.38 | 17.8 | 2.68 | 3.30 | 4.05 | 1.75 | 2.30 | 2.60 | 3.90 | 1.80 | 1.76 | 1 | 1 |
| 954.5 | 3131.5 | 2.28 | 21.1 | 2.62 | 3.70 | 4.11 | 1.83 | 2.35 | 3.40 | 4.12 | 1.94 | 1.75 | 0 | 1 |
| 1060.2 | 3478.5 | 2.53 | 13.4 | 2.76 | 3.75 | 4.20 | 2.16 | 2.43 | 3.60 | 4.30 | 1.67 | 1.73 | 1 | 0 |
| 1170.2 | 3839.2 | 2.38 | 17.0 | 2.66 | 3.45 | 4.00 | 1.94 | 2.41 | 3.15 | 4.00 | 1.73 | 1.66 | 1 | 1 |
| 1228.4 | 4030.1 | 2.61 | 5.1 | 2.70 | 4.45 | 4.90 | 2.31 | 2.46 | 4.12 | 4.70 | 1.88 | 1.99 | 1 | 0 |
| 1294.4 | 4245.9 | 2.67 | 6.3 | 2.79 | 4.90 | 5.30 | 2.65 | 2.99 | 4.62 | 5.30 | 1.80 | 1.77 | 0 | 0 |
| 1305.7 | 4283.8 | 2.49 | 10.4 | 2.66 | 4.35 | 4.95 | 2.60 | 3.00 | 3.60 | 4.95 | 1.60 | 1.65 | 1 | 1 |
| 1320.1 | 4331.0 | | | | 4.70 | 5.00 | | | 4.02 | 5.00 | | | 1 | 0 |
| 1415.9 | 4645.5 | 2.59 | 10.7 | 2.78 | 4.70 | 5.00 | 2.68 | 2.92 | 4.58 | 5.15 | 1.71 | 1.71 | 1 | 0 |
| 1837.0 | 6026.8 | 2.66 | 2.8 | 2.71 | 5.62 | 5.80 | 2.64 | 2.88 | 5.51 | 5.75 | 2.11 | 2.01 | 0 | 0 |
| 1984.6 | 6511.0 | 2.72 | 11.5 | 2.94 | 5.02 | 5.30 | 2.87 | 3.09 | 4.90 | 5.30 | 1.71 | 1.72 | 0 | 1 |
| 2226.6 | 7305.0 | 2.69 | 3.1 | 2.74 | 5.75 | 5.87 | 3.11 | 3.19 | 6.00 | 6.05 | 1.84 | 1.84 | 0 | 0 |
| 2618.4 | 8590.5 | 2.53 | 6.5 | 2.64 | 5.45 | 5.60 | 3.14 | 3.39 | 5.20 | 5.60 | 1.70 | 1.65 | 0 | 1 |

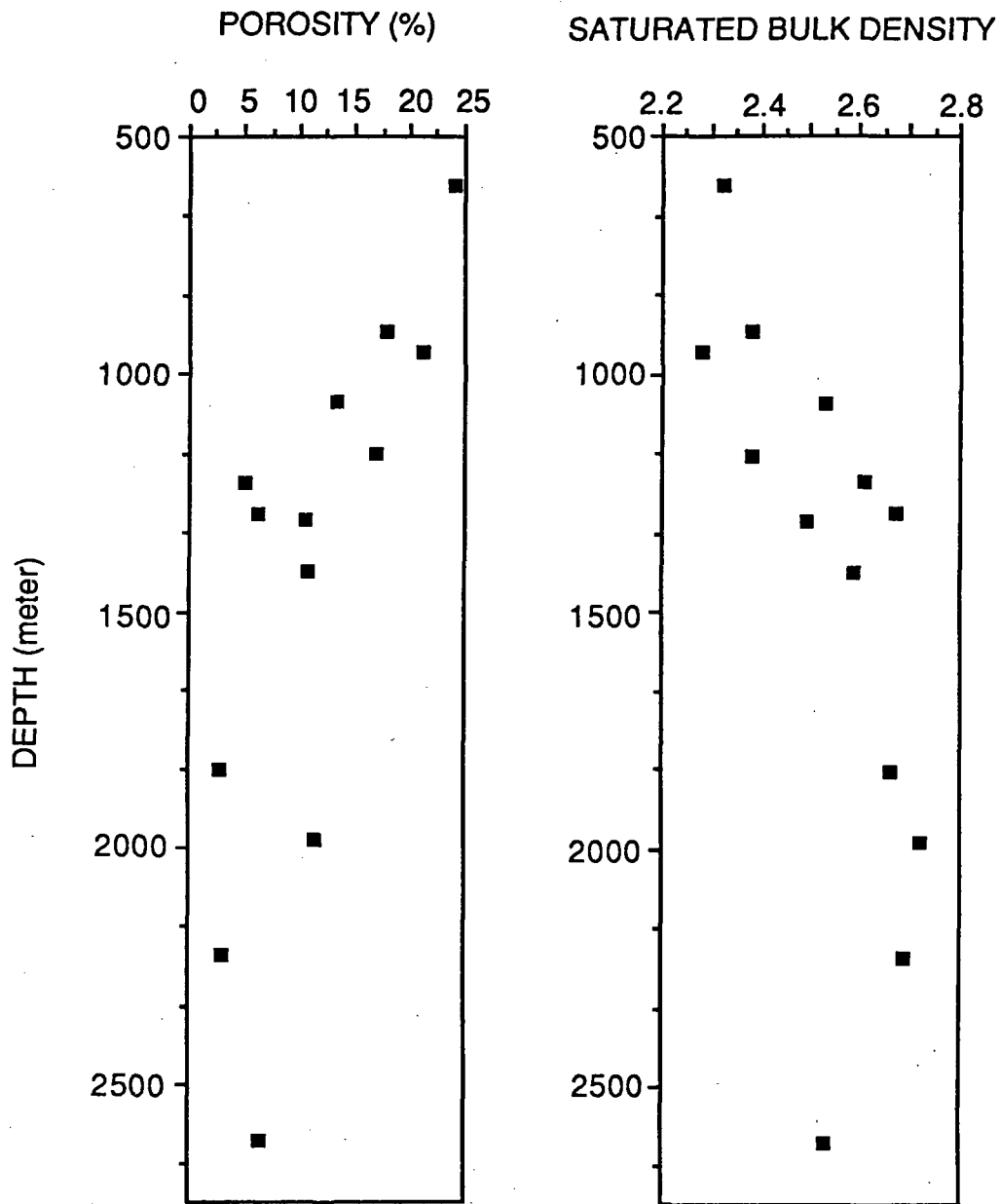
Table II - Table of the properties of the core samples.

- A: V_P at *in-situ* effective pressure measured on sample fully saturated with water.
- B: V_P at 200 MPa effective pressure measured on sample fully saturated with water.
- C: V_S at *in-situ* effective pressure measured on sample fully saturated with water.
- D: V_S at 200 MPa effective pressure measured on sample fully saturated with water.
- E: V_P at *in-situ* effective pressure measured on dry sample.
- F: V_P at 200 MPa effective pressure measured on dry sample.
- G: V_P/V_S at *in-situ* effective pressure measured on sample fully saturated with water.
- H: V_P/V_S at 200 MPa effective pressure measured on sample fully saturated with water.
- I: Orientation of the plug. 1 means plug axis is parallel to hole axis. 0 means plug cut normal to borehole axis.
- J: 1 means that the rock is classified as a sandstone. 0 means siltstone or shale.

| Depth (m) | Depth (feet) | Observations |
|-----------|--------------|------------------------------------------------------------------------------------------------------------------------------------------------------------------------------------------------------------------|
| 606.2 | 1988.7 | Mostly clays. Bedding visible, underlined with detrital quartz grains and anhydrite. Presence of rutile. |
| 911.0 | 2988.7 | Quartz grains and clays are predominant. A lot of pores are plugged with halide. |
| 954.5 | 3131.5 | Mostly quartz grains. Abundant clays. Presence of pyrite. Quartz grains: 65%. Pores + clays: 22%. K-feldspar: 12%. |
| 1060.2 | 3478.5 | Mostly clays. Bedding underlined with small (10 μ) quartz grains. |
| 1170.2 | 3839.2 | Mostly quartz grains: 78 %. Abundant calcite as pore-filling material. |
| 1228.4 | 4030.1 | Mostly clays. Detrital quartz grains throughout. |
| 1294.4 | 4245.9 | Mostly clays. Quartz grains: 12%. Quartz grains interspersed within surrounding bulky denser mineral of composition identical to composition of K-feldspar: 13%. halide: \cong 1%. |
| 1305.7 | 4283.8 | Detrital quartz: 60%. Detrital grains of K-feldspar or clays: 16%. Pores: 22%. |
| 1320.1 | 4331.0 | Mostly shale. Abundant small quartz grains (20 μ) throughout. |
| 1415.9 | 4645.5 | Small quartz grains surrounded by bulky mineral of composition identical to the composition of K-feldspar: 40%. Pores are abundantly filled with clays: 20%. Epidote fills the cracks and partly the pores: 40%. |
| 1837.0 | 6026.8 | Mostly silty clays (crystals a few microns wide). Abundant porosity: 20-30% |
| 1984.6 | 6511.0 | Quartz grains: 30%. Epidote filling the cracks and the pores: 30%. Quartz grains are interspersed in the surrounding epidote or clays. |
| 2226.6 | 7305.0 | Mostly silty clays. Detrital quartz throughout. |
| 2618.4 | 8590.5 | Mostly quartz: 91%. Epidote: 3%. pores: 5.5%. |

Table III - Table of the SEM observations.

It has not always been possible to give the mineralogical composition of the rock from the indications given by the Energy Dispersive System of the Scanning Electron Microscope.



Fig

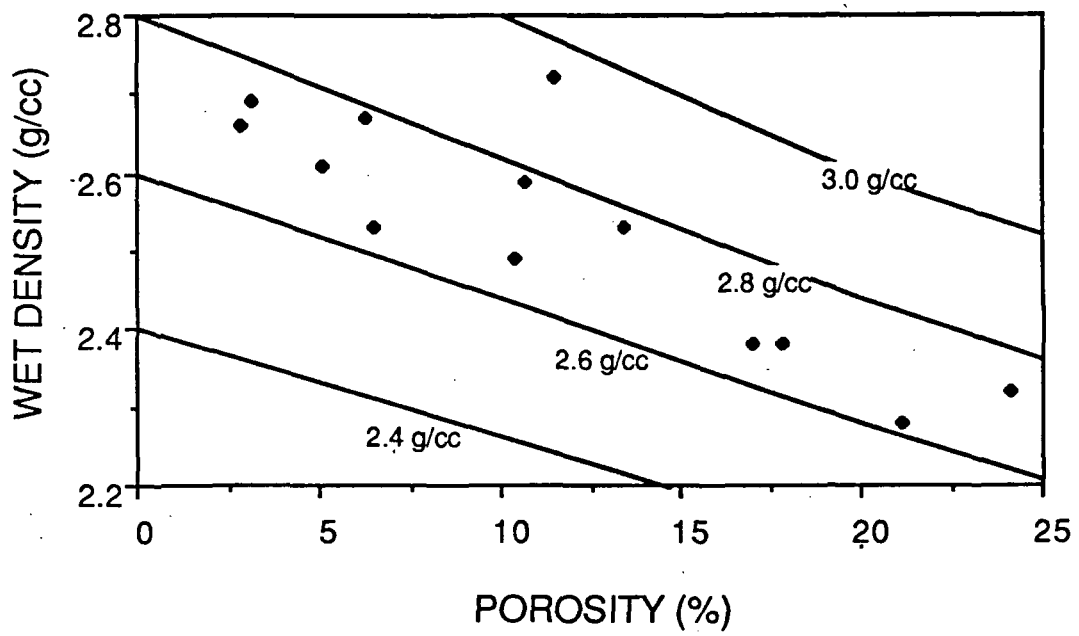


FIG 2

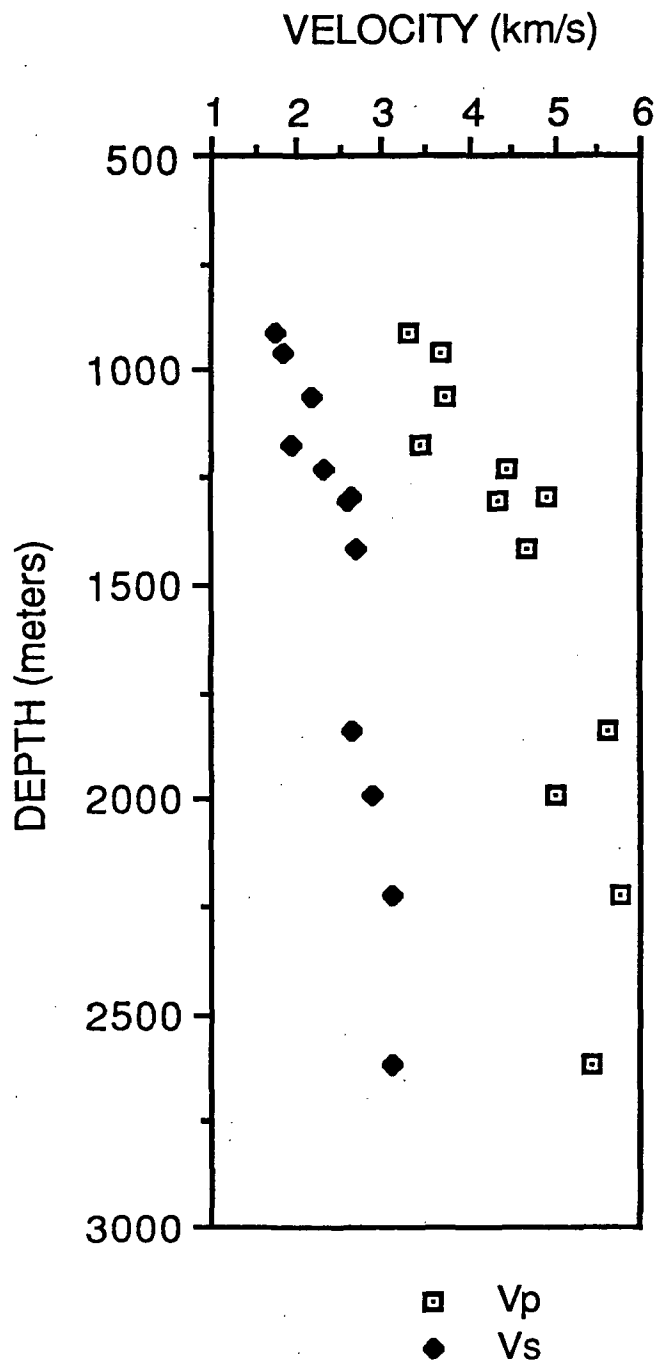


FIG 3

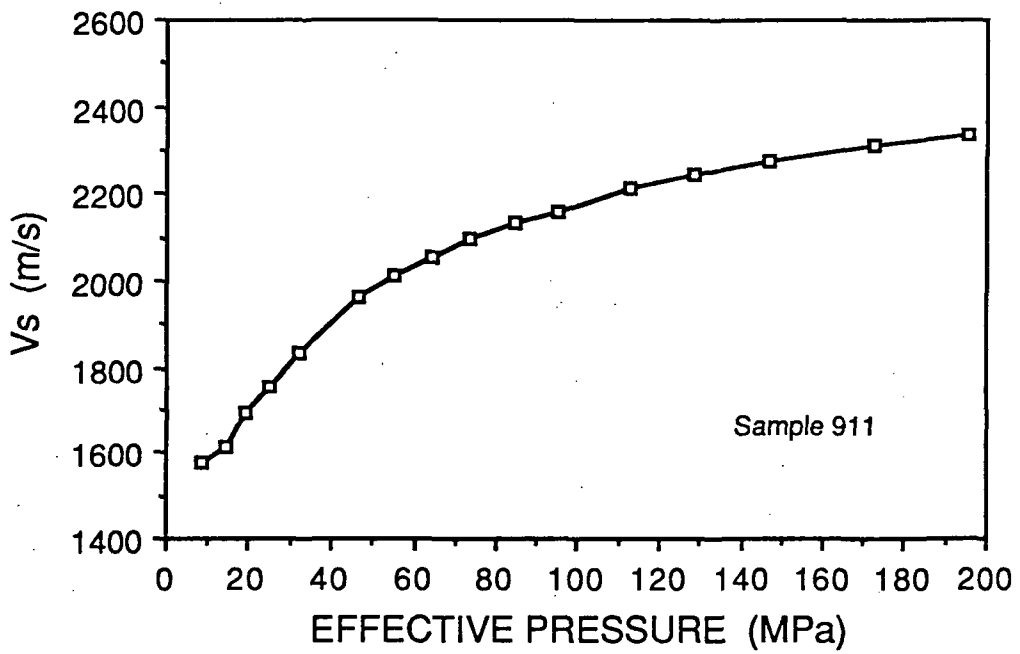
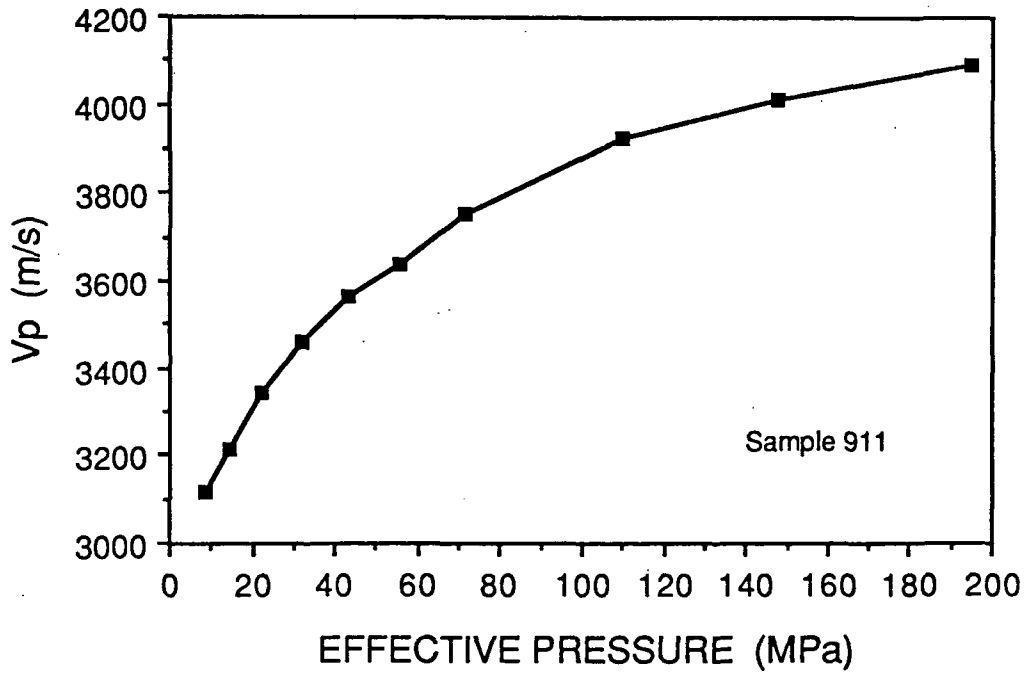
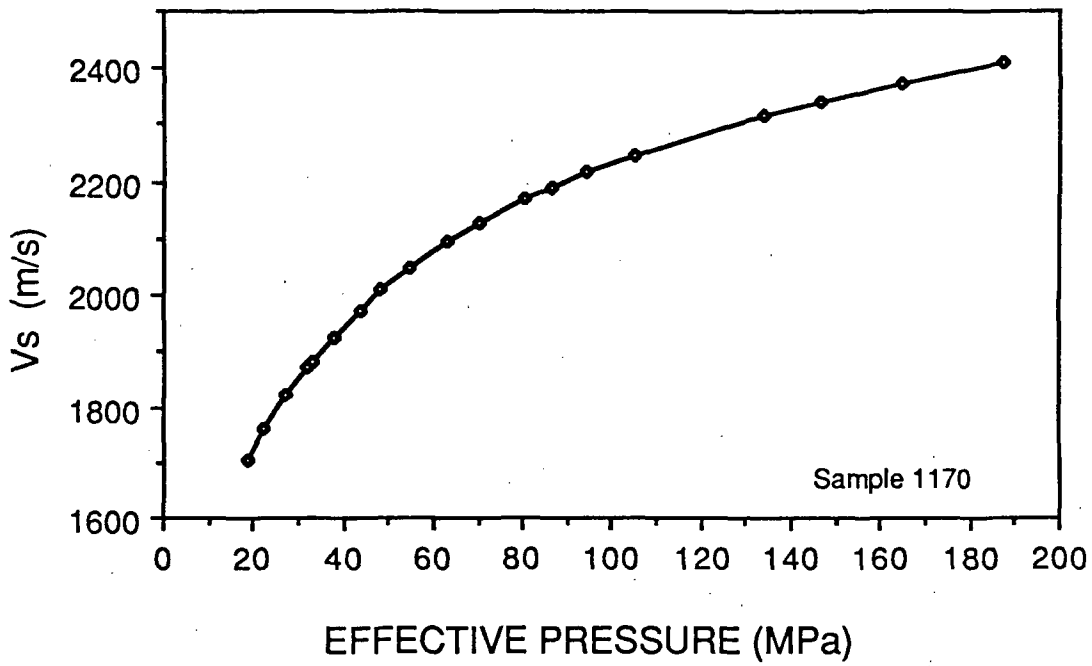
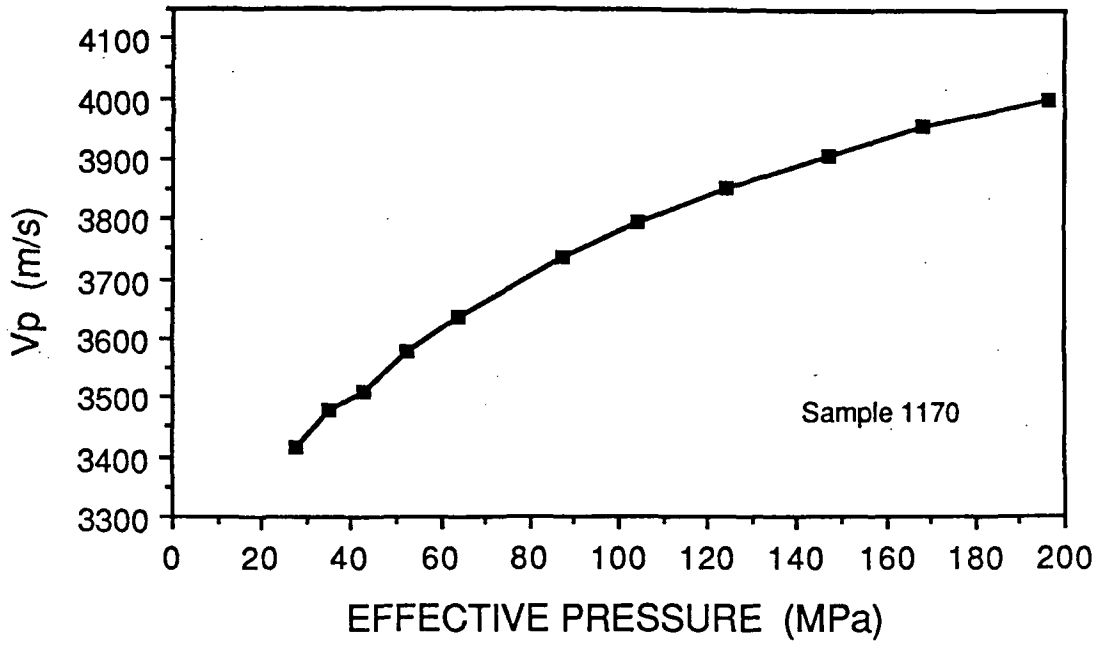
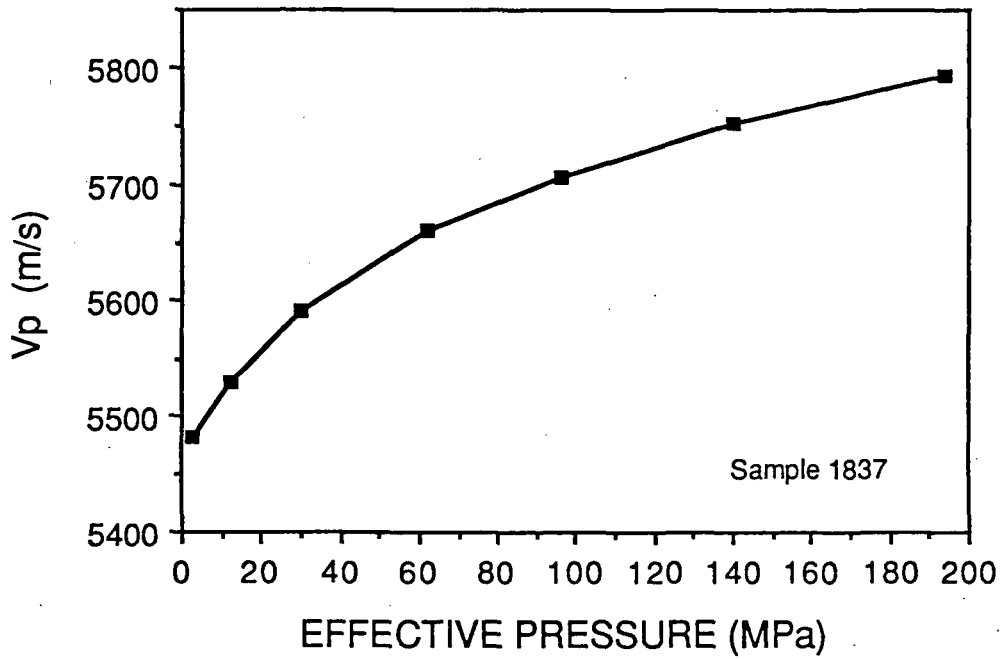
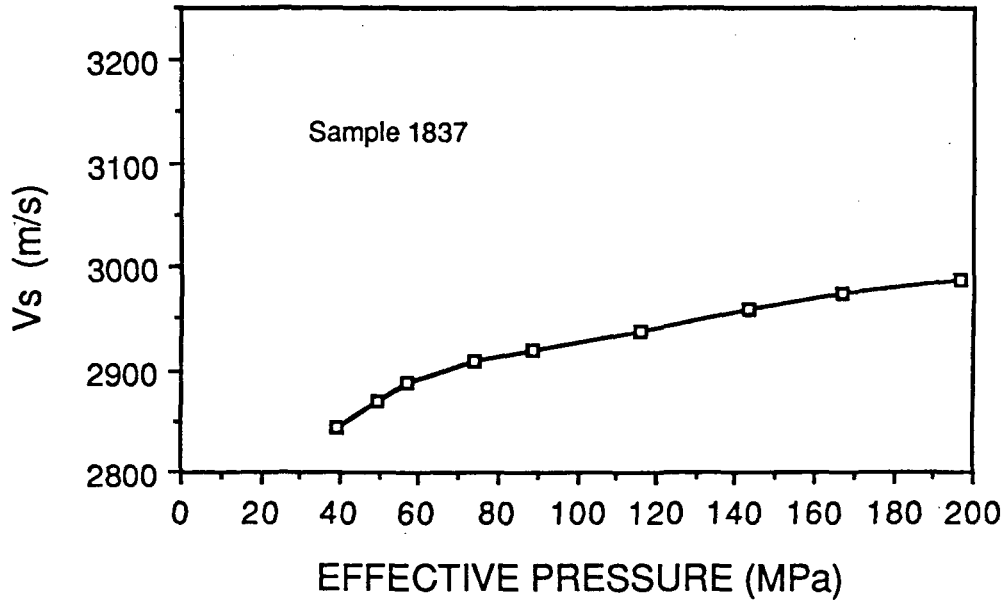


FIG. 1



27



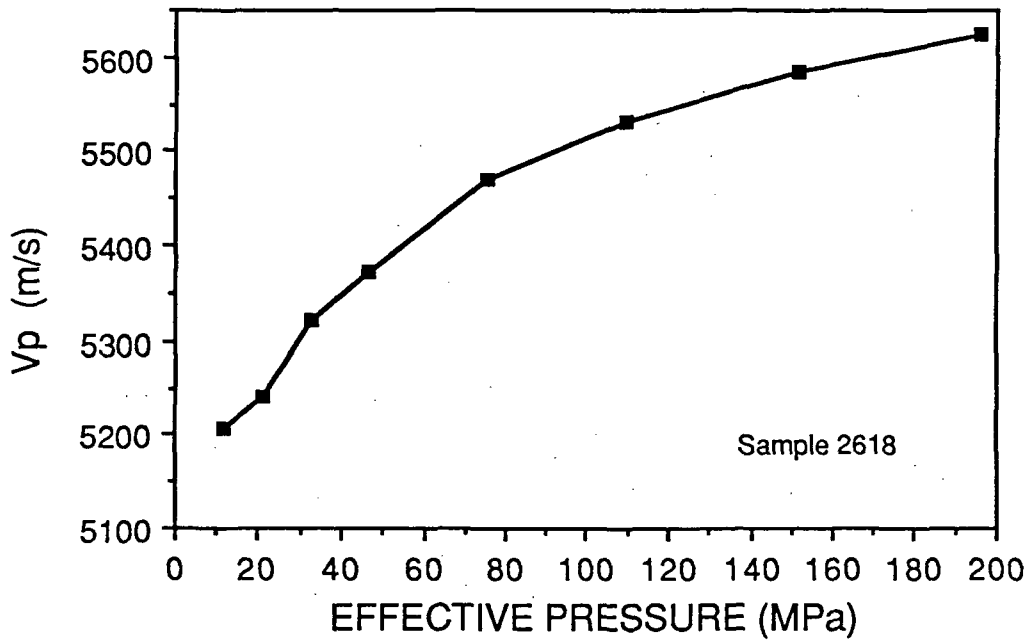
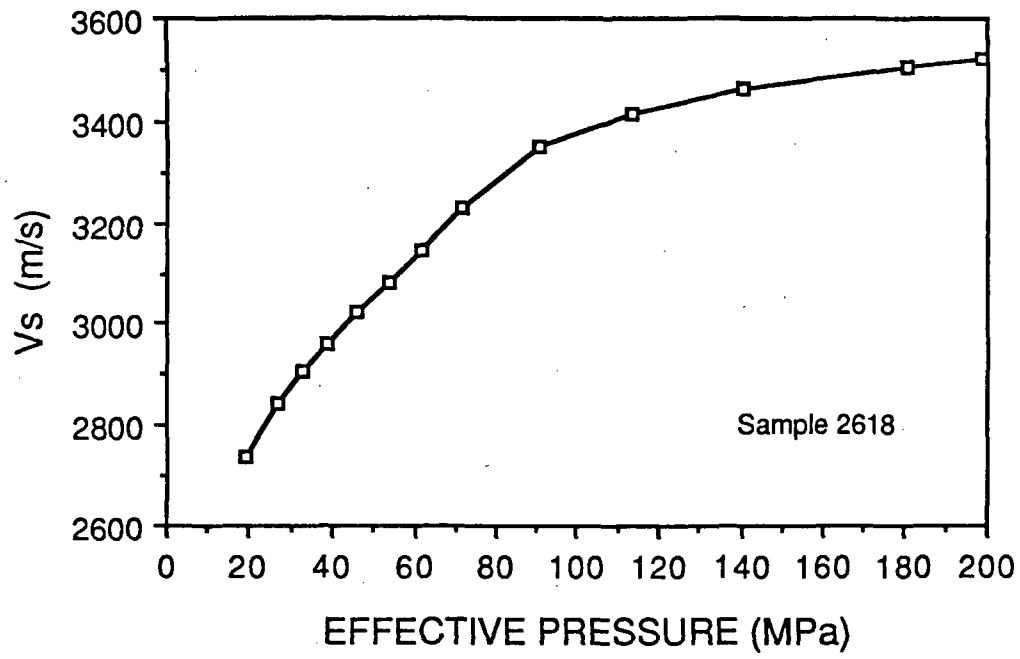


FIG 7

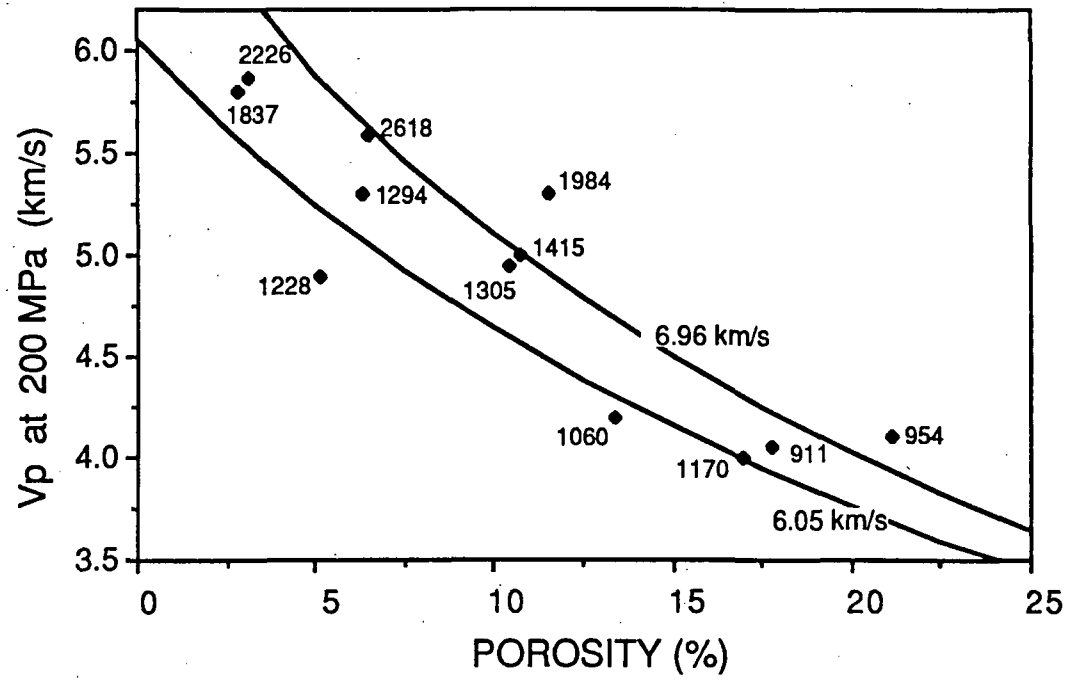


FIG 8

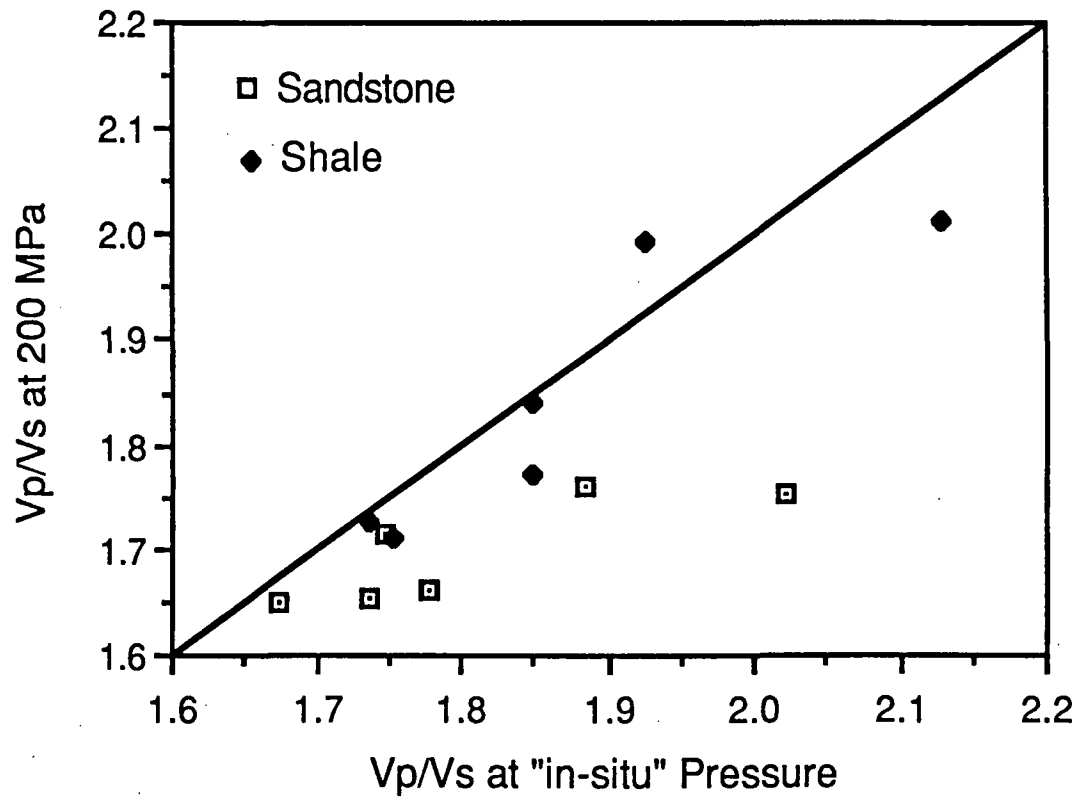


FIG 9

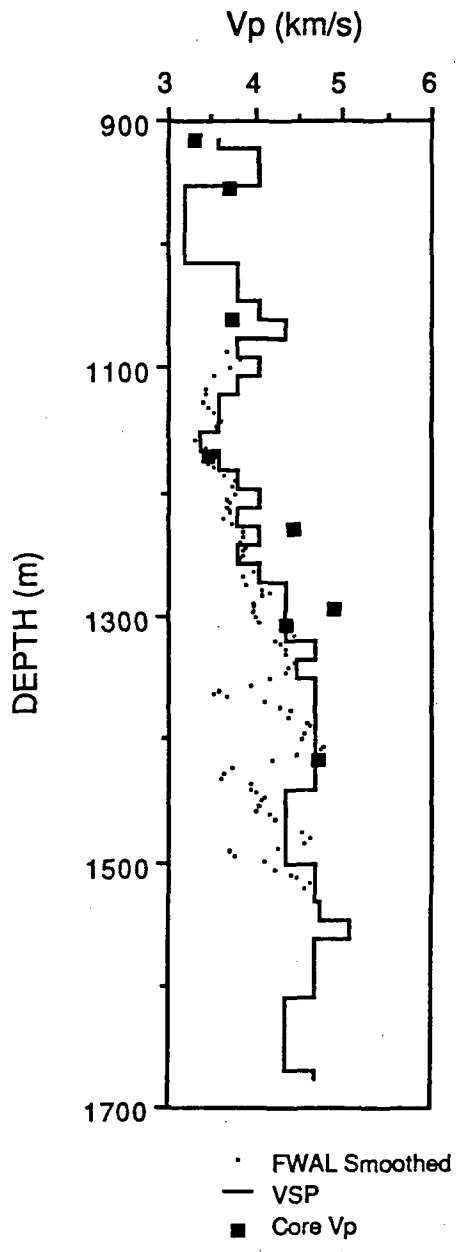
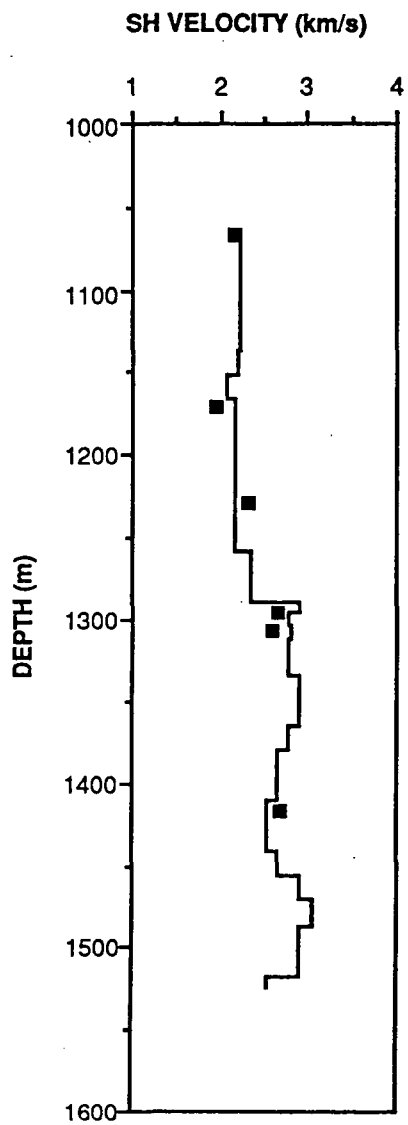
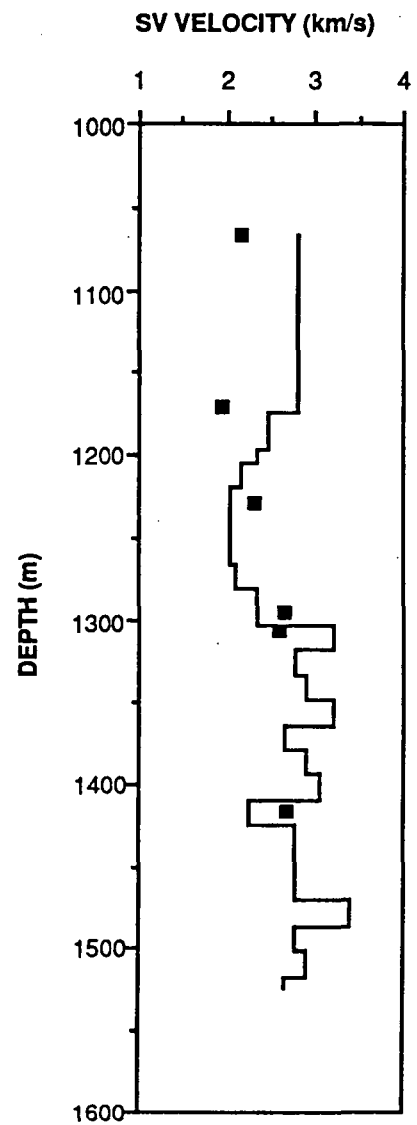


FIG 10



(a)

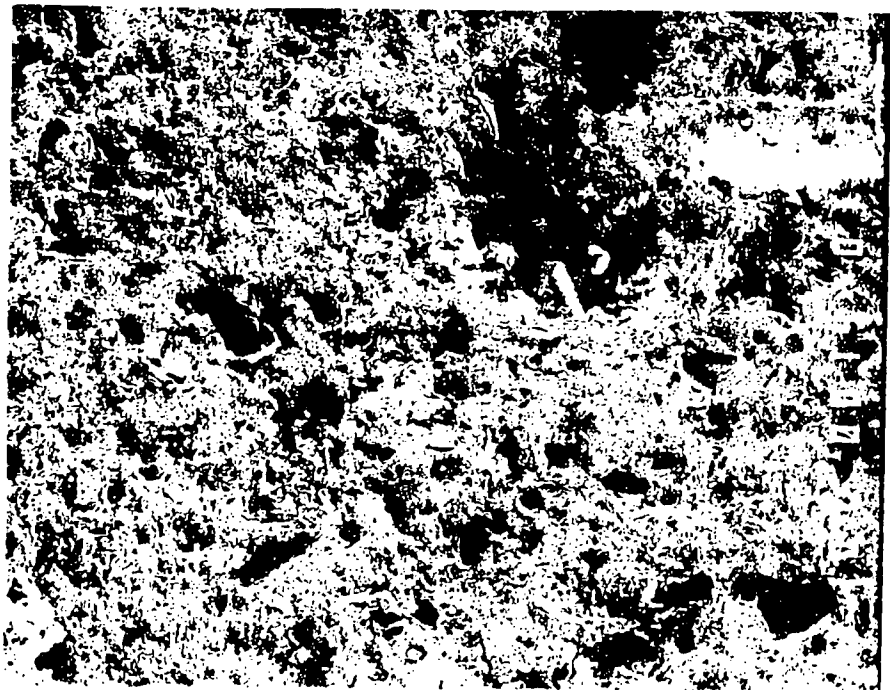


(b) ■ Vs Core



354

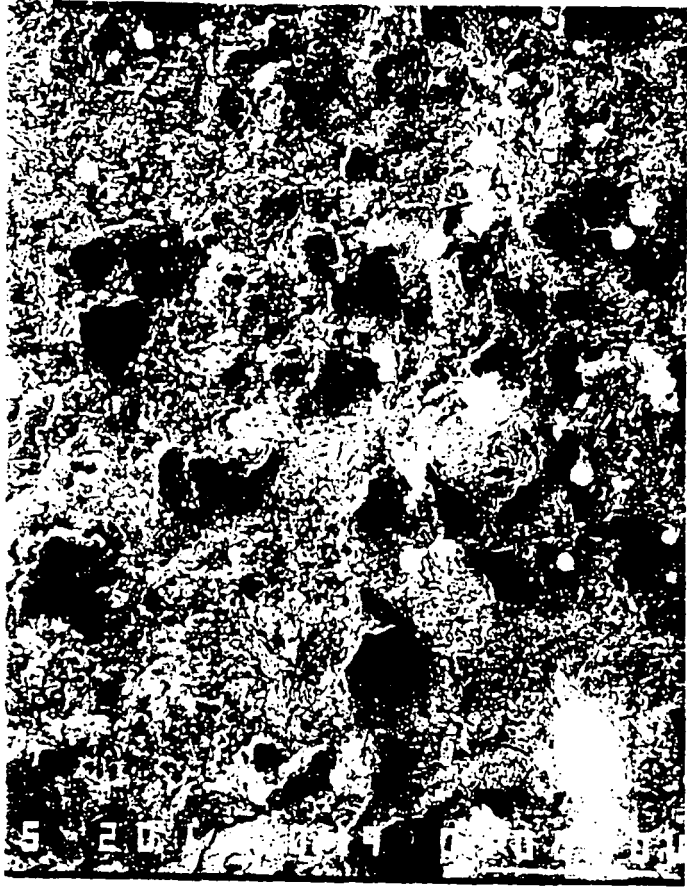
FlaFe 2



0901



1170



1228

MTGS



1294



1415



1984



2618

000008 V3:29